

State-space model of freely vibrating and surface-coupled cantilever dynamics in atomic force microscopy

Robert W. Stark*

Nanotechnology Group, Swiss Federal Institute of Technology Zurich, ETH Zentrum/CLA, CH-8092 Zurich, Switzerland

Georg Schitter

Nanotechnology Group, Swiss Federal Institute of Technology Zurich, ETH Zentrum/CLA, CH-8092 Zurich, Switzerland

Martin Stark

*Laboratoire de Spectrométrie Physique, UJF et CNRS, 140 rue de la physique, BP 87, F-38402 St Martin d'Hères Cedex, France
and Laboratoire d'Etudes des Propriétés Electronique des Solides, CNRS 25, Avenue des Martyrs, BP 166,
F-38042 Grenoble Cedex, France*

Reinhard Guckenberger

Max-Planck-Institut für Biochemie, Abteilung Molekulare Strukturbiologie, D-82152 Martinsried, Germany

Andreas Stemmer

Nanotechnology Group, Swiss Federal Institute of Technology Zurich, ETH Zentrum/CLA, CH-8092 Zurich, Switzerland

(Received 22 August 2003; revised manuscript received 17 November 2003; published 27 February 2004)

The dynamics of the microcantilever in atomic force microscopy (AFM) is represented by a multiple-degrees-of-freedom state-space model and is discussed within the framework of system theory. The cantilever dynamics is modeled as a linear time-invariant system with a nonlinear output feedback due to the tip-sample interaction. This allows one to use the same model to analyze different aspects of atomic force microscopy such as the dynamics of contact-mode or the dynamics of tapping-mode AFM. The state-space approach to the dynamic response of the AFM cantilever allows for numerically efficient simulations. We show that not only the eigenfrequency but also the modal damping of a cantilever interacting with a surface strongly depends on the contact stiffness. This is important for a quantitative characterization of elastic sample properties. Additionally, our model shows the presence of higher harmonics in tapping-mode AFM. The excitation of higher eigenmodes can strongly distort the system response. The results illustrate that higher eigenmodes have to be considered in the analysis of dynamic AFM.

DOI: 10.1103/PhysRevB.69.085412

PACS number(s): 68.37.Ps, 07.79.Lh, 07.05.Tp

I. INTRODUCTION

The different modes of dynamic atomic force microscopy (AFM) range from ultrasonic AFM with a permanent contact between tip and sample over the tapping mode with intermittent contact to the noncontact mode where mechanical contact is absent.¹ In the ultrasonic or acoustic mode the tip is in direct contact with the specimen while ultrasonic waves are coupled to the cantilever support or to the specimen. Analyzing the response of a surface-coupled cantilever^{2,3} in the frequency domain allows one to determine mechanical characteristics of the contact between tip and sample. The local stiffness can be measured by ultrasonic AFM,⁴⁻⁶ friction by acoustic friction force microscopy,^{7,8} and lateral stiffness by torsional overtone microscopy.⁹⁻¹¹

Another widely used dynamic AFM mode operates in intermittent contact and is also known as the tapping mode. Here, the freely oscillating cantilever is driven near or at its resonant frequency. For imaging, the vibrating tip is brought close to the sample surface as illustrated in Fig. 1. Thus, the oscillation of the cantilever is confined on one side by the sample surface that acts as a repulsive barrier defined by the elastic properties of the sample.¹²⁻¹⁴ The interaction between tip and sample gives rise to nonlinear dynamics. The exist-

ence of different oscillatory states in tapping-mode and non-contact AFM as well as their stability was investigated with numerical simulations. For a review see Ref. 15.

The micromechanical AFM cantilever is a distributed parameter system that can be understood as a multiple-degrees-of-freedom (MDOF) system allowing for a higher eigenmode excitation in tapping-mode AFM.¹⁶⁻¹⁹ Recently, we have shown that these higher-order signals provide direct access to the time-resolved measurement of tip-sample interaction forces.²⁰

In the following, we develop a MDOF state-space model of the AFM cantilever interacting with the specimen surface. This approach allows us to use an identical model in order to investigate the characteristics of a freely vibrating cantilever as well as those of a surface-coupled cantilever. Additionally, this model directly provides a theoretic understanding for the generation of higher harmonics by the nonlinearity in the contact between tip and sample in tapping-mode AFM.

II. MODELING

A. Modal analysis

The equation of motion for the transverse-displacement response $z(\xi, t)$ of a freely vibrating undamped cantilever beam is

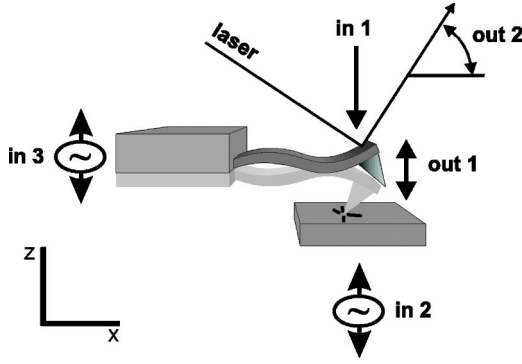


FIG. 1. Schematics of tapping mode AFM. Commonly used inputs and outputs of the dynamical system are indicated. The system can be accessed by applying forces directly onto the free end of the cantilever (input 1) by external forces like the tip-sample interaction or external actuation. Alternative inputs are base excitation of the sample (input 2) or excitation of the cantilever support (input 3). The tip deflection (output 1) determines the tip-sample interaction force. However, this output often cannot be observed directly. Most commonly, the angle of the cantilever deflection is read out using an optical lever detection scheme (output 2).

$$EI \frac{\partial^4 z(\xi, t)}{\partial \xi^4} + m \frac{\partial^2 z(\xi, t)}{\partial t^2} = 0, \quad (1)$$

with the normalized position $\xi \in [0, 1]$ along the cantilever, the time t , the flexural stiffness EI , and the constant mass per unit length, m . The resonant frequencies ω_n are related to the respective eigenvalues k_n by

$$\omega_n^2 = (k_n)^4 EI/m. \quad (2)$$

The modal shapes $\varphi(\xi)$ are determined by the boundary conditions. At the base side of the cantilever beam at $\xi=0$ the cantilever is clamped; i.e., the boundary conditions are $\varphi(0)=0$ for the displacement and $\varphi'(0)=0$ for the deflection slope. On the free end of the cantilever at $\xi=1$ the corresponding values are $\varphi''(1)=0$ and $\varphi'''(1)=0$. The eigenvalues of the free cantilever are determined by the characteristic equation

TABLE I. Summary of the output values of the n th mode for the tip position $\varphi_n(1)$ and the optical lever detection $\varphi'_n(1)$. Note the amplification of the modal response $\varphi'_n(1)$ as compared to $\varphi_n(1)$ due to geometric effects.

n	1	2	3	$n \geq 4$
$\varphi_n(1)$	-2	2	-2	$(-1)^n \times 2$
$\varphi'_n(1)$	-0.8763	3.0435	-4.9966	$\approx (-1)^n \times (2n-1)$

$$\cos k_n \cosh k_n = -1. \quad (3)$$

For higher modes the asymptotic value $k_n^{(a)} = (n - \frac{1}{2})\pi$ is a good approximation. Similar considerations lead to the characteristic equation of a clamped-pinned beam [$\varphi(1)=0$ and $\varphi''(1)=0$] corresponding to a cantilever that is supported by the surface

$$\cos k_n \sinh k_n + \sin k_n \cosh k_n = 0. \quad (4)$$

The eigenvectors (modal shapes) for the free cantilever are

$$\begin{aligned} \varphi_n(\xi) = & \cos k_n \xi - \cosh k_n \xi - \frac{\cos k_n + \cosh k_n}{\sin k_n + \sinh k_n} \\ & \times (\sin k_n \xi - \sinh k_n \xi). \end{aligned} \quad (5)$$

At the free end at $\xi=1$ one obtains the values of the modal displacement $\varphi_n(\xi)$ and the modal deflection angle $\varphi'_n(\xi)$ given in Table I.

B. Tip-sample interaction

In close proximity of a surface the attractive and repulsive regimes have to be discriminated. The attractive regime ($z_s - z \geq a_0$) can be described by an attractive van der Waals interaction force. Here, z is the tip deflection towards the sample and z_s the distance between the sample and tip of the undeflected cantilever. For systems without or with negligible energy dissipation in the tip-sample contact the tip-sample force can be calculated in the repulsive regime ($z_s - z < a_0$) using a Derjaguin-Müller-Toporov (DMT) model.²¹ This leads to

$$F_{ts}(z) = \begin{cases} -HR/[6(z_s - z)^2], & z_s - z \geq a_0, \\ -HR/6a_0^2 + \frac{4}{3}E^* \sqrt{R}(z_s - z + a_0)^{3/2}, & z_s - z < a_0, \end{cases} \quad (6)$$

where H is the Hamaker constant and R the tip radius. The parameter a_0 is the interatomic distance.²² The effective contact stiffness is given by $E^* = [(1 - \nu_t^2)/E_t + (1 - \nu_s^2)/E_s]^{-1}$, where E_t and E_s are the respective elastic moduli and ν_t and ν_s the Poisson ratios of tip and sample. For the numerical simulation typical parameters for the tapping mode with a silicon cantilever were chosen: $k = 10 \text{ Nm}^{-1}$, $R = 20 \text{ nm}$, $E_t = 129 \text{ GPa}$, and $\nu_t = 0.28$. A fused silica SiO_2 sample with $E_s = 70 \text{ GPa}$, $\nu_s = 0.17$, $a_0 = 0.166 \text{ nm}$, and $H = 6.4 \times 10^{-20} \text{ J}$ was assumed.

In the case of small oscillations around an equilibrium position z_0 —e.g., due to thermal excitation^{10,23,24}—the contact force relation, Eq. (6), can be linearized and expressed as an effective spring constant

$$k_{ts}^* = - \left. \frac{\partial}{\partial z} F_{ts}(z) \right|_{z=z_0} = \begin{cases} -HR/[3(z_s - z_0)^3], & z_s - z_0 \geq a_0, \\ 2E^* \sqrt{R}(a_0 + z_s - z_0)^{1/2}, & z_s - z_0 < a_0. \end{cases} \quad (7)$$

The contact stiffness k_{ts}^* is normalized to the cantilever spring constant k with $\hat{k}_{ts} = k_{ts}^*/k$. Notably, the van der Waals forces in the attractive regime lead to a negative effective spring constant.

C. State-space model

The physical system (Fig. 1) of the AFM cantilever and the nonlinear tip-sample interaction can be modeled as the combination of a linear time-invariant system (cantilever) with a nonlinear output feedback as illustrated in Fig. 2. In the following, only forces acting on the cantilever tip [input (1)] will be considered—i.e., the forces between tip and sample and the driving force. Experimentally, an external driving force at input (1) corresponds to a magnetic excitation of the cantilever. To focus the following discussion on the role of the specimen surface as an output feedback the extension of the model to multiple inputs will not be discussed here. The state-space form of the equations of motion of the cantilever with n degrees of freedom is

$$\dot{\mathbf{x}} = \mathbf{A}\mathbf{x} + \mathbf{b}u, \quad (8)$$

$$\mathbf{y} = \mathbf{C}\mathbf{x} + \mathbf{d}u, \quad (9)$$

with the time-dependent state vector $\mathbf{x} = (x_1, x_2, x_3, \dots) = (x_{i=1}, \dot{x}_{i=1}, x_{i=2}, \dot{x}_{i=2}, \dots)$; i.e., the state vector consists of the displacements and velocities of the respective degrees of freedom. The $2n \times 2n$ matrix \mathbf{A} is the system matrix, \mathbf{b} is the input vector, and scalar u is the force input. In the case of multiple inputs \mathbf{b} becomes a matrix and u a vector. Each component of the output vector \mathbf{y} —i.e., the tip displacement output y_1 and the photodiode signal output y_2 —are linear combinations of the states. The output matrix \mathbf{C} contains the respective weights. The direct transmission scalar \mathbf{d} is zero because there is no direct access from the force input (1) to the outputs (1) and (2) of the system.

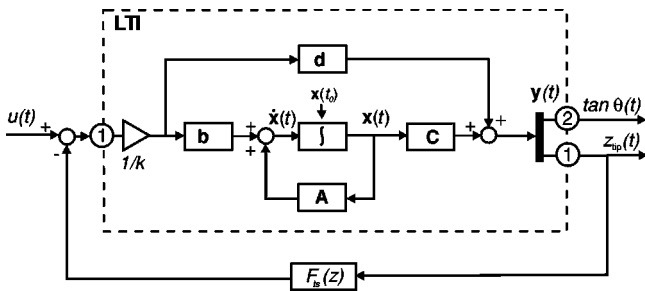


FIG. 2. Graphical representation for the state-space model of the AFM. The cantilever is represented by a linear and time-invariant (LTI) sub-model. The tip-sample interaction force is a nonlinear output feedback.

Under ambient conditions, the cantilever can be considered as a weakly damped system. Therefore, the uncoupled eigenmodes of the beam as obtained in the previous section can be used to construct the state-space model. The system matrix of the weakly damped free cantilever is given by the normalized eigenfrequency $\hat{\omega}_n = \omega_n/\omega_1$ and damping γ_n of each mode with a 2×2 submatrix along the diagonal. The input vector for forces acting on the tip contains the respective modal displacement φ_n at the geometric position of the force input ξ_{tip} , weighted with the respective generalized modal masses $M_i = \int_0^1 m \varphi_i(\xi)^2 d\xi$, leading to a rewritten Eq. (8):

$$\begin{bmatrix} \dot{x}_1 \\ \dot{x}_2 \\ \dot{x}_3 \\ \dot{x}_4 \\ \dots \end{bmatrix} = \begin{bmatrix} 0 & 1 & 0 & 0 & \dots \\ -\hat{\omega}_1^2 & -2\gamma_1\hat{\omega}_1 & 0 & 0 & \dots \\ 0 & 0 & 0 & 1 & \dots \\ 0 & 0 & -\hat{\omega}_2^2 & -2\gamma_2\hat{\omega}_2 & \dots \\ \dots & \dots & \dots & \dots & \ddots \end{bmatrix} \times \begin{bmatrix} x_1 \\ x_2 \\ x_3 \\ x_4 \\ \dots \end{bmatrix} + \begin{bmatrix} 0 \\ \varphi_1(\xi_{tip})/M_1 \\ 0 \\ \varphi_2(\xi_{tip})/M_2 \\ \dots \end{bmatrix} u. \quad (10)$$

Without restriction the mass density is normalized to $M_i = m = 1$. A uniform modal damping $\gamma_i = \gamma = 1/(2Q)$ is assumed in the following. The output matrix combines the states to the tip displacement and the photodiode signal with the output gains as given in Table I, leading to a new Eq. (9):

$$\begin{bmatrix} y_1 \\ y_2 \end{bmatrix} = \begin{bmatrix} \varphi_1(\xi_{tip})/n_{pos} & 0 & \varphi_2(\xi_{tip})/n_{pos} & 0 & \dots \\ \varphi_1'(\xi_{sens})/n_{sig} & 0 & \varphi_2'(\xi_{sens})/n_{sig} & 0 & \dots \end{bmatrix} \times \begin{bmatrix} x_1 \\ x_2 \\ x_3 \\ x_4 \\ \dots \end{bmatrix}. \quad (11)$$

With this definition, output y_1 is the geometric displacement of the cantilever at the tip location ξ_{tip} on the beam, whereas output y_2 is the deflection slope of the cantilever beam at the sensor position ξ_{sens} as measured by a light lever detection. In the following we assume the standard configuration with a read-out of the cantilever displacement and deflection angle at the free end of the cantilever at and $\xi_{tip} = \xi_{sens} = 1$. The output channels are normalized to the respective static gain.

Normalization of the deflection output (1) corresponds to the normalized quasistatic spring constant $\hat{k}_{\text{cant}}=1$ of the cantilever. The normalization of the light lever sensor output (2) corresponds to the usual quasistatic calibration of the photodiode response by measurement of a force versus displacement curve. The tip-sample interaction force is modeled as a static output feedback. The displacement of the tip, $y_1 = \sum_{i=1}^n x_{2i-1}$, is fed back through the interaction force $F_{\text{ts}}(y_1)$ to input (1) of the model. The following analysis will focus on how the sample stiffness affects system dynamics. For clarity, we will not consider velocity-dependent feedback components, e.g., due to viscous damping in the tip-sample contact or time variable interaction forces, e.g., due to capillary condensation or creep.

III. RESULTS AND DISCUSSION

A. Linearized model

To illustrate the influence of the output feedback on the dynamic system the linearized system of the AFM cantilever in contact with the specimen [Eq. (7)] is analyzed first.³¹ In this linear approximation the output feedback is directly proportional to the system's position output (1). Thus, the elastic surface properties can be conceived as a proportional feedback with the gain parameter \hat{k}_{ts} . From an experimental point of view, this is a useful approximation when the cantilever undergoes very small oscillations in a potential—e.g., due to thermal noise or due to a small excitation. Correspondingly, a dissipative interaction due to viscous sample properties could be represented by a differential feedback.

For the numerical calculations the quality factor was set to a typical value of $Q=200$ for all modes. The frequency response of the system for a relative tip-sample stiffness of $\hat{k}_{\text{ts}} = \pm 0.7$ [Eq. (7)] is given in Fig. 3. An attractive interaction corresponding to a spring with a negative force constant results in a shift to lower frequencies (dash-dotted line) as compared to the freely oscillating cantilever (dashed line). In contrast, a repulsive tip-sample interaction, corresponding to a spring with a positive spring constant, leads to a shift of the resonant frequencies to higher values (solid line). The resonant frequencies (given by the system poles) depend on the output feedback but are not affected by the choice of output channel. In contrast, the transmission zeros of the model are located differently for the position output (1) as compared to the light lever signal [out (2)]. The relative frequency shift of the higher-order modes is smaller as compared to the fundamental mode because the frequency shift depends on the stiffness ratio $\hat{k}_{\text{ts}}/m\hat{\omega}_i^2$, which rapidly decreases with increasing mode number i .

Increasing the effective tip-sample stiffness further to $\hat{k}_{\text{ts}} = 10^5$ the system approximates a cantilever with its end pinned to the sample surface (Fig. 4). The poles of the constrained system are the transmission zeros (antiresonances) of the displacement output (1) of the free system.²⁵ This means that the resonance frequencies of the strongly surface coupled cantilever correspond to frequencies of the minimal displacement response of the free cantilever. In the position output (1) the cantilever response shows a constant gain

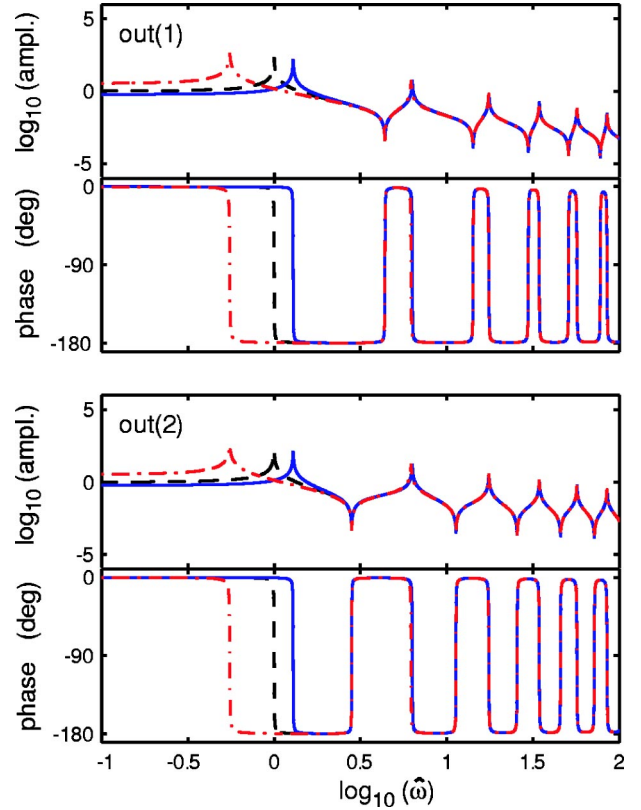


FIG. 3. (Color online) Amplitude and phase response of the free (dashed, black) and weakly surface coupled cantilever from input (1) to the outputs as indicated. The solid line (blue) corresponds to a repulsive interaction with $\hat{k}_{\text{ts}}=0.7$. The dash-dotted line (red) represents $\hat{k}_{\text{ts}}=-0.7$, which is an attractive interaction corresponding to a spring with negative force constant.

since the poles migrate to the stationary zeros and are canceled. Since the zeros in the photodiode signal (2) differ from the zeros in the position output (1), they are not canceled in output (2) and the resonances can still be observed.

A root locus map allows a very compact representation of the migration of the system's poles and zeros. The map in Fig. 5 visualizes the respective variations of eigenfrequency and damping as a result of changes of the effective tip-sample stiffness \hat{k}_{ts} —i.e., the feedback parameter. Shown are the positions of poles and zeros of the subsystem from input (1) to the tip-position output (1). The position of the poles and zeros of the free cantilever in the Laplace plane are indicated by crosses and circles, respectively. For the free cantilever all poles are located in the left half plane; i.e., the dynamic system is stable.

In this model the number of zeros, n_{zero} , is determined by the number of poles, $n_{\text{poles}}=2n$, with $n_{\text{zero}}=n_{\text{poles}}-2$, because the position of the force input ξ_{tip} and the sensor position ξ_{sens} are the same. This collocated configuration is generally desirable in AFM. For an in-depth discussion of the role of poles and zeros and the collocation of sensor and actuator in mechanical systems see Ref. 25. For the usual single-degree-of-freedom approximation ($n=1$) the system does not have any zeros. The zeros remain stationary since they are independent from \hat{k}_{ts} for the given structure A, b, C , and d .

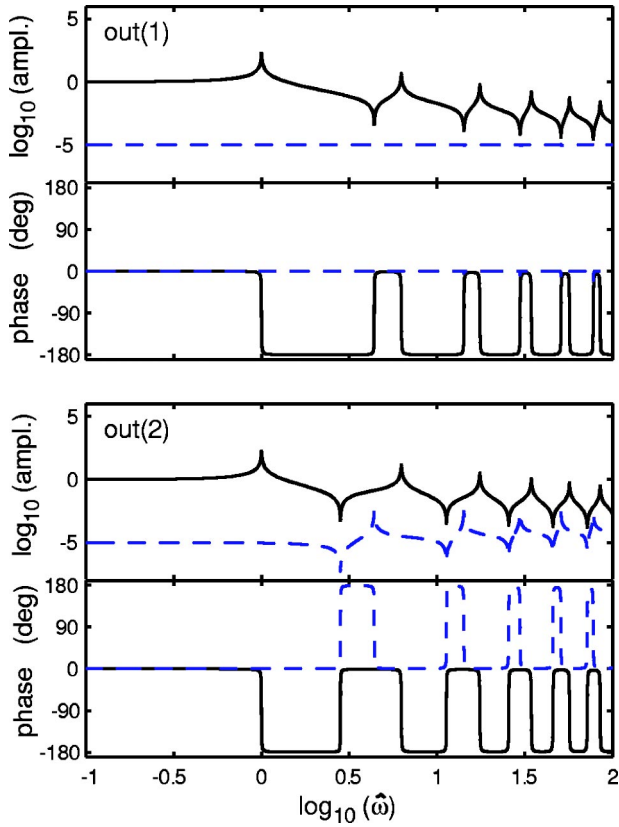


FIG. 4. (Color online) Bode plot of the free (solid line, black) and strongly surface-coupled cantilever ($\hat{k}_{ts}=10^5$, dashed line, blue). Output (1): tip displacement; output (2): photo diode signal.

In the positive imaginary half-plane the migration path of the poles towards the zeros is indicated for a tip-sample stiffness $\hat{k}_{ts} \in [0, 1e10]$. Because poles and zeros are either complex conjugate pairs or real values, the respective conjugate complex migration paths are not shown in Fig. 5. For an infinite contact stiffness poles and zeros cancel except for the complex conjugate highest-order poles that diverge. The ar-

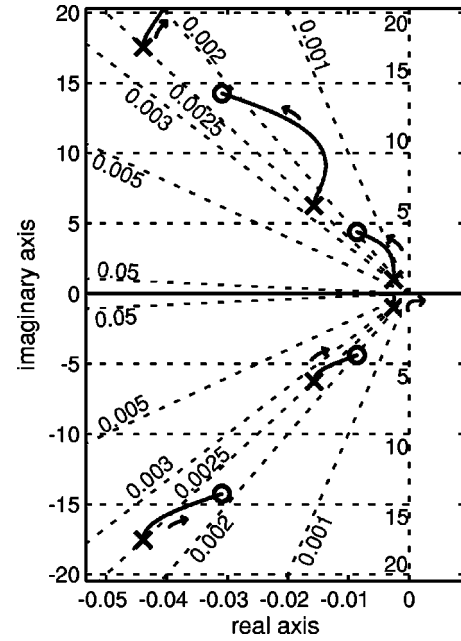


FIG. 5. Root locus map of the linearized closed loop system in the Laplace plane. For better representation the real axis was stretched significantly. The locations of equal damping appear as diagonal lines in this plot with the respective damping as indicated. Poles and zeros are indicated by crosses and circles, respectively. In the positive imaginary half-plane the migration of the poles due to feedback by a positive spring constant is illustrated by the solid curves. The arrows give the direction of the pole migration for increasing $\hat{k}_{ts} > 0$. The zeros remain stationary. In the negative imaginary half-plane the pole migration due to feedback by a negative spring constant (attractive regime) is illustrated for decreasing $\hat{k}_{ts} < 0$.

rows indicate the direction of migration for an increasing \hat{k}_{ts} . It is most important to note that also the modal damping varies substantially due to increasing stiffness of the tip-sample contact. For the first eigenmode the damping can be

TABLE II. Summary of the absolute values of the eigenvalues for the n th mode of the closed loop system for different values of the effective tip-sample stiffness \hat{k}_{ts} . The eigenvalues for the pinned system are obtained by directly solving the characteristic equation. Corresponding values for an intermediate sample stiffness can be found in Ref. 2. For comparison the data for systems with selected DOF are given.

DOF	n	$\hat{k}_{ts} = -0.1$	Free	0.1	1	10	1e10	Pinned
1	1	1.8264	1.8751	1.9203	2.2299	3.4149	592.96	3.9266
	2	1.8275	1.8751	1.9191	2.2159	3.1932	3.9721	3.9266
3	2	4.6912	4.6941	4.6970	4.7237	5.0199	700.73	7.0686
	1	1.8276	1.8751	1.9190	2.2143	3.1754	3.9405	3.9266
	2	4.6912	4.6941	4.6970	4.7235	5.0063	7.1602	7.0686
30	3	7.8541	7.8548	7.8554	7.8610	7.9203	774.88	10.2102
	1	1.8277	1.8751	1.9189	2.2135	3.1677	3.9267	3.9266
	2	4.6912	4.6941	4.6970	4.7234	5.0011	7.0689	7.0686
	3	7.8541	7.8548	7.8554	7.8610	7.9190	10.2111	10.2102
	4	10.9953	10.9955	10.9958	10.9978	11.0185	13.3538	13.3518
	5	14.1371	14.1372	14.1373	14.1382	14.1479	16.4972	16.4934

reduced from the value of the free system ($\gamma=0.25\%$ at $\hat{k}_{ts}=0$) by factor of more than 2 ($\gamma=0.11\%$ at $\hat{k}_{ts}=9$) due the surface coupling. Increasing the tip-sample stiffness beyond this damping minimum leads to an increased damping until a value of $\gamma=0.2\%$ is obtained at $\hat{k}_{ts}=1e10$. These variations of the modal damping have to be taken into account when viscoelastic properties of the specimen are determined from analysis of the frequency response of a surface coupled cantilever or a cantilever that is coupled to a molecule. The intrinsic damping obtained by an active Q -control force spectroscopy experiment²⁶ is the intrinsic damping of the entire dynamic system.

In the negative imaginary half-plane of Fig. 5 the migration of the poles is illustrated for $\hat{k}_{ts} \in [0, -1e10]$. The paths of the respective conjugate complex poles are not shown. The arrow indicates the direction of migration for a decreasing negative \hat{k}_{ts} . The poles migrate towards zeros with lower frequency. For $\hat{k}_{ts} < -m\omega_1^2 = -1$ one of the dominant poles becomes real and positive and the system becomes unstable. Experimentally, this instability is well known as “snap-in” in AFM.²⁷ When a soft cantilever is approached closely to the surface at a certain point the cantilever suddenly bends to the surface due to the attractive van der Waals forces. Within the framework of this model the “snap-in” can be understood as an instability of the closed loop system. Due to this instability, the system transits through the attractive part of the potential and ends up in the repulsive regime where it is stable again.

To evaluate the numerical convergence of the state-space approach the absolute values of the eigenvalues of the different systems are summarized in Table II for different model orders n . The columns “free” and “pinned” correspond to solutions of the characteristic equations (3) and (4). Already with $n=3$ modes the relative error of the first eigenvalue is $<1\%$ at $\hat{k}_{ts}=1e10$ as compared with the analytic solution for the pinned cantilever. The errors can be reduced by increasing the number of modes further. With $n=30$ modes an accuracy of the first five eigenvalues of 0.01% is achieved. The eigenvalues of the highest-order modes of the respective model diverge for strong surface coupling—i.e., for large spring constants. The single-degree-of-freedom system ($n=1$) approximates the fundamental mode of a weakly surface coupled cantilever well but fails to adequately describe a strongly surface coupled cantilever.

B. Nonlinear model

The dynamics of the tapping mode was simulated using the nonlinear DMT model of the tip-sample interaction in Eq. (6). The computational time needed for the simulations depends on the model order of the system. With increasing model order the computational time per time step is augmented with n^2 , where n is the number of eigenmodes. To capture the dynamics of higher modes at reasonable computational costs a cantilever model with three modes was assumed resulting in a sixth-order state-space model.

The system was driven by a sinusoidal signal in input (1) at the fundamental resonance ω_1 of the system. The ampli-

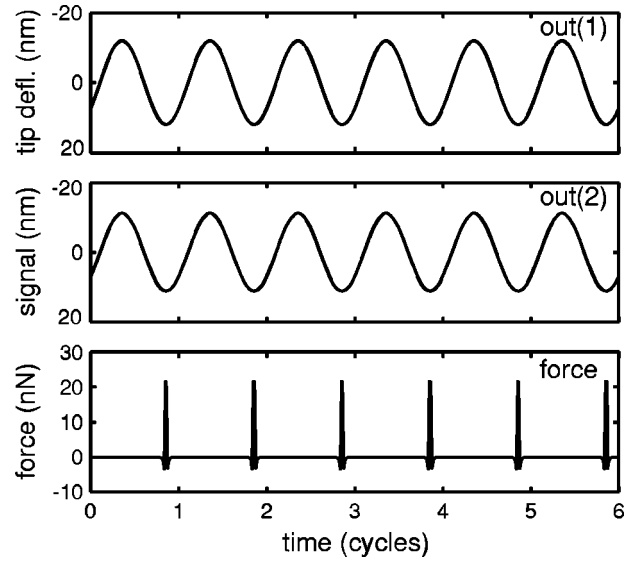


FIG. 6. Time series of the steady state response of the system in tapping mode at a sample position of 12 nm and the corresponding interaction force between tip and sample. The signals in tip deflection output (1) and the photo diode output (2) are nearly sinusoidal.

tude of the driving force was set to $F=1$ nN corresponding to a free amplitude of about $A_0=20$ nm. These are typical conditions for imaging in ambient conditions. In order to simulate the tapping mode, the distance between the sample and tip’s rest position was reduced. First, the dynamics at a distance of $z_s=12$ nm which corresponds to an amplitude setpoint of $A/A_0 \approx 60\%$ was investigated. After waiting for the equilibration of the system a time series of output data (six cycles) was extracted (Fig. 6). Both output signals—the tip displacement and photodiode signal—are nearly sinusoidal. The tip-sample forces are single impacts at the lower turning point of the tip oscillation. The time of repulsive contact between tip and sample is 3% of the cycle time. The repulsive interaction with peak forces of 23 nN indicates that the system is in the so-called high-amplitude state.¹⁵

For a further analysis the Fourier transform of the output signals was calculated using the fast Fourier transform (FFT) algorithm. In Fig. 7 the absolute values of the FFT of the time series data of both outputs are shown. In both spectra harmonics of the driving frequency prevail. Additionally, the signature of the amplitude response of the respective output channel can be seen. The maxima are at the same frequencies for both output channels at the 1st and around the 6th and 18th harmonics that are close to the resonant frequencies. However, the minima are different. The displacement [out(1)] minima are close to the 4th and 15th harmonics whereas in the light lever signal [out(2)] the minima are close to the 3rd and 12th harmonics. Although the cantilever deflection has a spectral minimum at the 4th and 15th harmonics the signal does not vanish in out(2). Here, it is important to note the physical difference between both output channels. The output channel (1) is connected to the system input (1) via the mechanical feedback due to the tip-sample interaction, whereas output (2) only serves as a read-out.

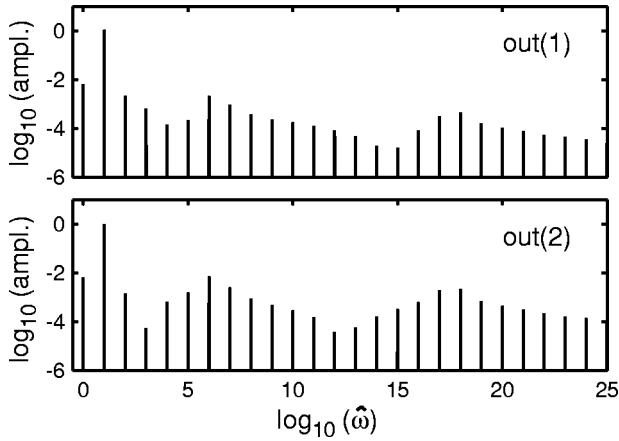


FIG. 7. Absolute values of the fast Fourier transformation of the time series data. The spectrum consists of harmonics of the driving frequency in both signals, tip deflection output (1) and photo diode output (2). The harmonics are generated by the nonlinearity in the tip-sample contact. For visualization, both channels are normalized to the respective fundamental harmonic.

To measure the fraction of power transferred into higher harmonics by the nonlinear processes the respective total harmonic distortion (THD) as observed in both output signals was calculated. It provides a measure for the fraction of power transferred into higher harmonics of a signal by nonlinear processes. It can be defined as the root-mean-square (rms) value of the sum of the higher harmonics of the output signal $y_{i,n}$ of output i , divided by the rms value of the sum of all harmonics (including the fundamental signal $y_{i,1}$) of the respective output channel:

$$\text{THD}_i = \frac{\sqrt{\sum_{n=2}^{\infty} y_{i,n}^2}}{\sqrt{\sum_{n=1}^{\infty} y_{i,n}^2}}. \quad (12)$$

The harmonic distortion is a function of the amplitude set-point. For the position outputs it is $\text{THD}_1 = 2.0\%$ and for the light lever output $\text{THD}_2 = 2.3\%$ at $z_s = 12$ nm. In the output (2) the harmonic distortion is increased as compared to output (1) due to the geometric amplification of the higher modes in the light lever detection (cf. Table I).

The generation of higher harmonics is due to the nonlinearity of the tip-sample interaction. The higher harmonics as well as the dc contribution depend on the frequency response of the respective cantilever output and on the interaction force between tip and sample. Since a time-independent tip-sample interaction was assumed, the equations of motion can be normalized in time, scaling with the fundamental resonance of the cantilever. The normalized spectra of the system outputs, and thus the absolute values of the higher harmonics, do not depend on the numerical value of the cantilever's resonant frequency.

Another important question regarding the system dynamics is the influence of higher eigenmodes. The phase portraits

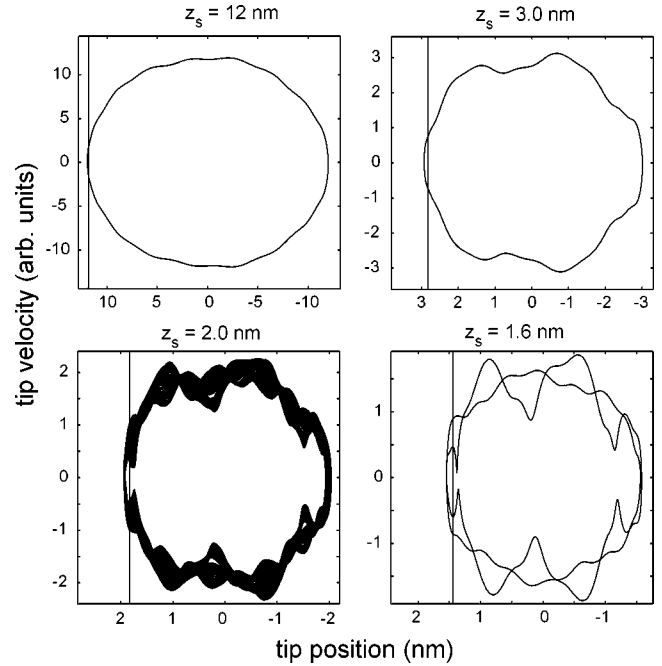


FIG. 8. Phase space trajectories of the tip [out (1)] for different sample positions as indicated. For the respective plots a trajectory with a length of 128 cycle times of the fundamental frequency was taken. The vertical line indicates the minimum of the surface forces in Eq. (6).

of output (1) shown in Fig. 8 and a computer animation³² illustrate this aspect. The evolution of the tip trajectory in phase space was calculated for distances in the range from $z_s = 22.9$ nm to $z_s = 0.1$ nm in steps of 0.1 nm. The system was allowed to equilibrate for 1152 cycles of the fundamental oscillation. Then, a trajectory of 128 cycles of the equilibrated system was used in order to generate the phase-space plot. The vertical line indicates the minimum of the DMT potential at $z_s - a_0$. On the right side of this line the tip-sample interaction is attractive, to the left it is repulsive.

Four phase portraits were selected as examples (Fig. 8). At a distance of $z_s = 12.0$ nm the phase-space trajectory is only weakly disturbed by higher-order oscillations. The system dynamics is dominated by the fundamental mode as could be expected from the THD value. However, approaching further to $z_s = 3.0$ nm the oscillation becomes strongly disturbed. Here, the higher eigenmodes become important for the system dynamics. At a distance of $z_s = 2.0$ nm the system shows a more complicated dynamics and the trajectory fills a larger portion of the phase space. In close proximity to the sample at $z_s = 1.6$ nm period doubling prevails. A weakly disturbed cycle is followed by a strongly disturbed cycle.

We have experimentally observed similar shapes of phase-space trajectories earlier employing a V-shaped cantilever (Fig. 4 in Ref. 17). However, so far, a rigid theoretical explanation was missing. The usual single degree-of-freedom approximations well described the dynamics at large distances^{14,28-30} z_s but failed to predict distorted phase-space trajectories at small distances. In another set of experiments we have also observed period doubling [Fig. 5(a,v) in

Ref. 20]. Again, the single-DOF approximations could not explain the tip trajectory exhibiting strong higher-order vibrations. From the results in Fig. 8 it is clear that the high-frequency oscillations are due to the excitation of higher eigenmodes of the cantilever. Thus, we conclude that at close proximity of the tip to the sample the additional degrees of freedom due to higher eigenmodes of the microcantilever play a vital role for the dynamics and cannot be neglected in numerical simulations.

IV. CONCLUSIONS

We have shown that the dynamic system consisting of the cantilever and the tip-sample interaction in atomic-force microscopy can be represented as a linear and time-invariant system with a nonlinear output feedback. This closed-loop system predicts well the dynamic response of the free and surface-coupled cantilever as well as the dynamics of tapping-mode AFM. Thus, the dynamic response of the surface-coupled cantilever is calculated efficiently and in a straightforward manner without the need of solving the full partial differential equation.

For very small excitation amplitudes a linearized interaction force between tip and sample can be assumed. The shift of the resonance frequencies of the cantilever interacting with a repulsive or attractive surface potential can be explained in terms of migrating poles due to the output feedback. In order to describe this effect correctly a multiple-degrees-of-freedom description of the cantilever is essential. It is shown that the modal damping of the surface coupled

cantilever strongly depends on the contact stiffness, even in the absence of contact damping. This system intrinsic effect is especially important for a quantitative characterization of the viscoelastic properties of the specimen—for example, in ultrasonic force microscopy or in mechanical AFM spectroscopy of single molecules. Additionally, the linearized model readily explains the snap-in of the tip onto the sample as an instability of the closed-loop system.

In the case of larger vibration amplitudes the full nonlinear interaction between tip and sample has to be considered. The model explains the generation of higher harmonics in the output signals of tapping-mode AFM in terms of a nonlinear output feedback. The calculations demonstrate that the values of the individual higher harmonics in the output signal as well as the respective total harmonic distortion depend on the output channel—i.e., on the signal readout. We show that for the investigation of the dynamics of tapping-mode AFM higher eigenmodes cannot be neglected.

In summary, the dynamic response of the AFM cantilever in ambient conditions can be modeled efficiently by a state-space model. The main advantage of conceiving the tip-sample interaction as a nonlinear output feedback is the possibility to study the complex dynamics of different AFM modes from contact-mode AFM over the tapping mode to ultrasonic mode within one unified model.

ACKNOWLEDGMENT

M.S. gratefully acknowledges financial support by the Alexander von Humboldt Foundation (Germany).

-
- *Current address: University of Munich, Section of Crystallography, Theresienstrasse 41, 80333 Munich, Germany. Fax: +49-89-2180-4334. Electronic address: stark@nanomanipulation.de
- ¹G. Friedbacher and H. Fuchs, *Pure Appl. Chem.* **71**, 1337 (1999).
 - ²U. Rabe, K. Janser, and W. Arnold, *Rev. Sci. Instrum.* **67**, 3281 (1996).
 - ³J.A. Turner, S. Hirsekorn, U. Rabe, and W. Arnold, *J. Appl. Phys.* **82**, 966 (1997).
 - ⁴K. Yamanaka, H. Ogiso, and O. Kolosov, *Appl. Phys. Lett.* **64**, 178 (1994).
 - ⁵U. Rabe and W. Arnold, *Appl. Phys. Lett.* **64**, 1493 (1994).
 - ⁶O. Kolosov, M. Castell, C. Marsh, and A. Brix, *Phys. Rev. Lett.* **81**, 1046 (1998).
 - ⁷K. Wahl, S. Stepanovski, and W. Unertl, *Tribol. Lett.* **5**, 103 (1998).
 - ⁸V. Scherer, W. Arnold, and B. Bhushan, *Surf. Interface Anal.* **27**, 578 (1999).
 - ⁹T. Drobek, R.W. Stark, M. Gräber, and W.M. Heckl, *New J. Phys.* **1**, 15.1 (1999).
 - ¹⁰T. Drobek, R.W. Stark, and W.M. Heckl, *Phys. Rev. B* **64**, 045401 (2001).
 - ¹¹M. Reinstädler, U. Rabe, V. Scherer, U. Hartmann, A. Goldade, B. Bhushan, and W. Arnold, *Appl. Phys. Lett.* **82**, 2604 (2003).
 - ¹²N. Burnham, O. Behrend, F. Ouvevey, G. Gremaud, P. Gallo, D. Gourdon, E. Dupas, A. Kulik, H. Pollock, and G. Briggs, *Nanotechnology* **8**, 67 (1997).
 - ¹³L. Nony, R. Boisgard, and J.P. Aimé, *J. Chem. Phys.* **111**, 1615 (1999).
 - ¹⁴S. Lee, S. Howel, A. Raman, and R. Reifengerger, *Phys. Rev. B* **66**, 115409 (2002).
 - ¹⁵R. García and R. Pérez, *Surf. Sci. Rep.* **47**, 197 (2002).
 - ¹⁶R.W. Stark and W.M. Heckl, *Surf. Sci.* **457**, 219 (2000).
 - ¹⁷M. Stark, R.W. Stark, W.M. Heckl, and R. Guckenberger, *Appl. Phys. Lett.* **77**, 3293 (2000).
 - ¹⁸O. Sahin and A. Atalar, *Appl. Phys. Lett.* **79**, 4455 (2001).
 - ¹⁹T.R. Rodríguez and R. García, *Appl. Phys. Lett.* **80**, 1646 (2002).
 - ²⁰M. Stark, R.W. Stark, W.M. Heckl, and R. Guckenberger, *Proc. Natl. Acad. Sci. U.S.A.* **99**, 8473 (2002).
 - ²¹B.V. Derjaguin, V.M. Muller, and P. Toporov Yu, *J. Colloid Interface Sci.* **53**, 314 (1975).
 - ²²R. García and A. San Paulo, *Phys. Rev. B* **61**, R13 381 (2000).
 - ²³J. Cleveland, T. Schäffer, and P. Hansma, *Phys. Rev. B* **52**, R8692 (1995).
 - ²⁴R.W. Stark, T. Drobek, and W.M. Heckl, *Ultramicroscopy* **86**, 207 (2001).
 - ²⁵D.K. Miu, *Mechatronics* (Springer, Heidelberg, 1993).
 - ²⁶A.D.L. Humphris, J. Tamayo, and M.J. Miles, *Langmuir* **16**, 7891 (2000).
 - ²⁷H.O. Hao, A.M. Baró, and J.J. Saenz, *J. Vac. Sci. Technol. B* **9**, 1323 (1991).
 - ²⁸N. Sasaki, M. Tsukada, M. Tamura, R. Tamura, K. Abe, and N.

Sato, Appl. Phys. A: Mater. Sci. Process. **66**, S287 (1998).

²⁹J. Hunt and D. Sarid, Appl. Phys. Lett. **72**, 2969 (1998).

³⁰R.W. Stark, G. Schitter, and A. Stemmer, Phys. Rev. B **68**, 085401 (2003).

³¹The numerical simulations were implemented in MATLAB release 13 and SIMULINK.

³²See EPAPS Document No. E-PRBMDO-69-018408 for an

animation (animated gif) that shows the evolution of the phase space trajectory. A direct link to this document may be found in the online article's HTML reference section. The document may also be reached via the EPAPS homepage (<http://www.aip.org/pubservs/epaps.html>) or from <ftp.aip.org> in the directory /epaps/. See the EPAPS homepage for more information.